Development of alumina microspheres with controlled size and shape by vibrational droplet coagulation

Reference:

Pype Judith, Michielsen Bart, Seftel Elena, Mullens S., Meynen Vera.- Development of alumina microspheres with controlled size and shape by vibrational droplet coagulation

Journal of the European Ceramic Society / European Ceramic Society - ISSN 0955-2219 - (2016), p. 1-10

Full text (Publishers DOI): http://dx.doi.org/doi:10.1016/j.jeurceramsoc.2016.07.020

Development of alumina microspheres with controlled size and shape by vibrational droplet coagulation

J. Pype[a,b*], B. Michielsen[a], E. M. Seftel[a,b], S. Mullens[a], V. Meynen[b]

[a] Sustainable Materials Management, Flemish Institute for Technological Research NV – VITO NV, Boeretang 200, 2400 Mol, Belgium

[b] Laboratory of Adsorption and Catalysis (LADCA), Department of Chemistry, University of Antwerp, CDE, Universiteitsplein 1, 2610 Wilrijk, Belgium

* Corresponding author: Judith.pype@vito.be

Abstract

Monodisperse alumina microspheres were shaped by making use of the vibrational droplet coagulation technique. A combination of both physical and chemical parameters provided a flexible basis to widely regulate the size of the microspheres. The controlled granulation is based on a stable alumina suspension containing sodium alginate. The sodium alginate binder is used to coagulate the microspheres jetted into a bath of $CaCl_2$. Several parameters have been varied to study the impact on the suspension's rheology. This in turn dictates the physical parameters required for controlled shaping by the vibrational droplet coagulation technique. The decomposition of the calcium alginate in the alumina microspheres was monitored during the thermal post processing. In this step, the formation of $CaCO_3$ was revealed, resulting in the presence of CaO during the calcination process. Subsequently, this existence of CaO in the alumina matrix leads to the formation of calcium hexaluminate ($CaO.6Al_2O_3$) during sintering.

Keywords: Alumina, microspheres, vibrational droplet coagulation, physical and chemical control, calcium alginate coagulation

1. Introduction

Ceramic microspheres are widely used in a broad range of applications [1]-[4], all with their own demands concerning the ideal correlation between properties versus performance, required in the processes. For example, when applied as catalysts or catalyst supports in fluidized bed reactions, their mechanical attrition resistance is strongly influenced by their uniform spherical shape and narrow size distribution, respectively [5]. Furthermore, the uniform size and shape together with a fine control of the porosity features are also essential when using the ceramic microspheres as sorbent materials in packed bed columns reactions [6]. All of the microsphere applications have in common that the size will have an impact on the performance. In order to comply with these different requirements depending on its application, the granulation needs to offer good control of the microspheres properties. Many granulation methods have been developed over the past decades such as spray drying [7], extrusion dripping [8], complex coacervation [9], interfacial polymerization [10] and vibrational droplet coagulation [11], all with their own benefits and limiting process parameters. According to Whelehan et al. [12] the different encapsulation techniques to create spherical particles can be divided in three categories, based on the force controlling the shaping technique: mechanical (spray drying and extrusion-based methods), physicochemical (complex coacervation) and chemical (interfacial polymerization) processes. Mechanical controlled encapsulation techniques have the advantage that they can easily control the size and shape of the produced microspheres. One example is the vibrational droplet coagulation, where a suspension or solution is dripped through a vibrating nozzle. By making use of an external force in the form of a vibration with defined frequency, the extruded liquid is broken up in droplets when it is passed through the nozzle. This way, it is possible to enhance the size control and productivity of the shaped microspheres in contrast to the extrusion dripping where the process is driven by a gravitational force [13][14]. Additionally, a coagulation mechanism is applied to chemically fixate the structure in the droplet shape. This coagulation mechanism adds an extra dimension of control to the shaping process and the final properties of the material, allowing a very broad structural and physicochemical

control of the obtained materials. This technique has already been applied for the controlled shaping process of silica xerogel microspheres [15][16] and alginate-silica hybrid materials for separation purposes [17]. However, the relationship between suspension composition and control of shaping was not elucidated.

The droplet generation in the process of vibrational droplet coagulation is determined by two parameters: the composition of the ceramic suspension and the physical parameters of the shaping process. Both define the shaping process and process window itself and affect at the same time also the final properties of the microspheres and are hence closely interrelated. In order to shape the microspheres, the suspension has to contain different components allowing solidification of the droplets. Therefore, besides inorganic particles dispersed in the solvent, sodium alginate is applied as a binder to solidify the droplets by means of the ionotropic gelation. Sodium alginate is a naturally occurring polysaccharide, consisting of two monomers: 1,4-linked β-D-mannuronic (M) and α-L-guluronic (G) acid residues. The sodium alginate is capable of forming a rigid three-dimensional structure as a result of the interactions of the guluronic acid residues with divalent or trivalent ions [18]. Moreover, as the shaping process is controlled by the laminar flow of the suspension through the nozzle, the viscosity of the alumina suspension has to be controlled. Typically ceramic suspensions exhibit a non-Newtonian relation resulting in shear-thinning behaviour at high shear rate [19][20].

The present study deals with the preparation of α-Al_2O_3 microspheres. Sodium alginate has been applied in combination with α-Al_2O_3 for gelcasting alumina shapes[21][22][23], where direct casting can be induced by calcium iodate $Ca(IO_3)_2$ [24]. In this case, all kind of shapes have been casted but the use of the iodate salt induces the gelation only over longer timespans. Since the shaping of microspheres requires an immediate reaction to retain the spherical shape, gelling agents with higher complexation kinetics are required. It is reported that the use of other Ca^{2+} salts such as

chlorine or nitrates, instantaneously complex with the alginate polymeric chains and consequently produces a rigid network on the droplet surface, which is maintaining the spherical shape [25] .

Recent work on shaping of alumina microspheres by extrusion dripping indicates an influence of calcium on the densification while sintering [13]. The alumina grain distribution after sintering shows the presence of needle like grains in the matrix of the microspheres. These results indicate that the presence of Ca^{2+} ions has an impact upon sintering the obtained microspheres. Nevertheless, a systematic elucidation of the influence of the suspension composition on the materials properties has not yet been reported.

A substantial amount of work has been reported in literature on the influence of the experimental parameters on the vibrational droplet technology in alginate systems [26][27][28]. However, none of these effects have been transferred to the ceramic loaded vibrational droplet technology. Nevertheless, some work has already been done on the incorporation of alumina in an alginate loaded system, a technology combining these two processes has not yet been demonstrated. Here we show how a combination of both physical and chemical parameters provides a flexible basis to broadly regulate the size and shape of the dense alumina microspheres in the granulation process. In addition, the boundaries of the system are explored, based on the knowledge of the pure alginate system. Calcium is inherent present due to the ionotropic gelation mechanism. Therefore, its impact on the sintering process is studied in detail. Different alumina suspensions are used in the research to link the alginate and powder content in the suspension to the resulting characteristics of the sintered microspheres. In this way, it is possible to tune the microsphere characteristics by controlling both the physical and the chemical parameters in the shaping and the sintering processes.

2. Materials and methods

2.1. Materials

α-alumina (A16 SG) was purchased from Almatis with a d_{50} of 0.5 µm and specific surface area of 9 m^2/g. Two different sodium alginate types were supplied by Brace GmBH (Alzenau, Germany): sodium alginate Br-W (low viscosity denoted as LA) and sodium alginate Br-GM (high viscosity denoted as HA). Furthermore, calcium chloride (Sigma Aldrich, anhydrous, powder ≥97 % pure), precipitated calcium carbonate (Acros organics, >99 % pure), ammonium polymethacrylate dispersing agent (Darvan C, Vanderbilt Minerals, Norwalk, CT), isopropyl alcohol (98 %) and RO water (<5 µS/cm) were used in this work.

2.2. Preparation of the ceramic suspensions and solidification bath

The preparation of the ceramic suspension can be divided in 3 steps. At first the alumina powder was dispersed in RO water with 0.5 wt% Darvan C. In order to eliminate agglomerates in the alumina slurry, grinding balls (3 mm yttrium stabilized zirconia in ratio 2:1 powder/grinding balls) were added and the dispersion is kept in motion on the rolling bench for several hours. Secondly, a sodium alginate solution (4 wt% in water) and extra RO water was added to the alumina slurry. The various prepared alumina suspensions are denoted in Table 1 showing the variations in powder and alginate content and the alginate type.

The solidification bath, containing the reacting salt to establish an ionotropic gelation, was made by dissolving 4 wt% calcium chloride in tap water. Isopropyl alcohol was sprayed on top of the coagulation bath to reduce its surface tension.

Table 1: Ceramic suspension composition for different alumina slurry's

Suspension	Powder loading (wt%)	Type of alginate	Alginate loading (wt%)
20P/0.56LA	20	LA	0.56
20P/0.66LA	20	LA	0.66
20P/0.88LA	20	LA	0.88
20P/0.88HA	20	HA	0.88
40P/0.66LA	40	LA	0.66
40P/0.88LA	40	LA	0.88
20P/1.48LA	20	LA	1.48

2.3. Shaping microspheres

The alumina microspheres were shaped by making use of the Spheronisator M (Brace GmbH, Alzenau Germany). The apparatus was set up as presented in Figure 1. The ceramic suspension was loaded in the feed tank, which contained a magnetic stirrer to prevent powder sedimentation during the process. By applying a constant pressure on the feed tank, a laminar flow was obtained through the nozzle. Following Rayleigh's jet instability theory [12][29], the flow was broken up in uniform droplets by applying a vibration with a defined frequency (185-2050 Hz) and amplitude (1500-3000 mV). A stroboscopic lamp was set at the same phase of the frequency as used at the nozzle, in order to visualize the falling droplets. The droplets were collected and solidified in the coagulation bath. The obtained solid microspheres were kept in the coagulation bath overnight to complete the solidification. Afterwards, the microspheres were thoroughly washed with tap water followed by RO water to remove the excess of ions and finally isopropyl alcohol to reduce capillary pressure during drying. The samples were dried at 80 °C, calcined (1h) at 600 °C and sintered (1h) at 1540 °C or 1650 °C (heating rate 2 °C/min) under ambient air and pressure conditions.

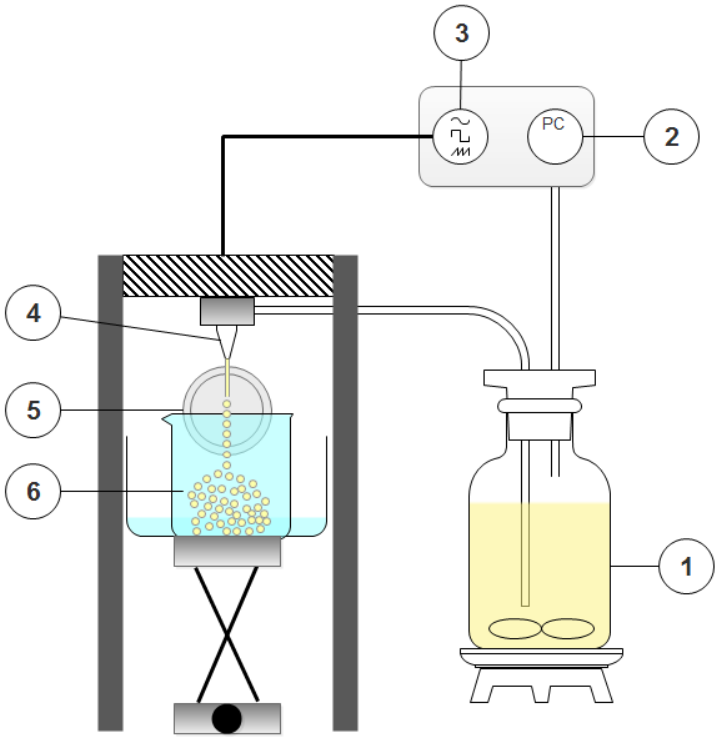

Figure 1: Schematic representation of the vibrational droplet coagulation set-up. (1) Feed vessel with magnetic stirrer; (2) Air pressure controller; (3) Vibration generator with frequency and amplitude control; (4) Nozzle; (5) Stroboscopic lamp; (6) Coagulation bath

2.4. Characterization techniques

The rheology of the alumina containing suspension was measured with a Haake mars rheometer (Germany, cup Z43 DIN 53018 and rotor Z41 DIN 53018). Rheology curves were provided in a shear rate interval between 0.1 and 1000 $^{s-1}$ and data points are collected when decreasing the shear rate. Viscosity screening in the shear rate interval took 7.5 minutes. The temperature was controlled by a thermostatic bath set at 25 °C.

The size distribution and sphericity of the obtained microspheres were measured by optical microscopy using a Zeiss Discovery V12 stereomicroscope, equipped with a Plan Apo S 1.0x FWD 60 mm objective. Images are taken by an Axiovision MRc digital camera connected to the microscope. Image processing was performed by Axiovion Rel. 4.8 software. The raw images were processed to obtain a binary image containing individual particle silhouettes by subtracting the background [8].

The image analysis was performed on at least 200 microspheres. The analysis was performed in wet, dry and sintered stage to obtain information about the shrinkage of the microspheres.

The feret ratio (or aspect ratio) is one of the most used shape factors in various applications to determine the sphericity of microspheres [30][31][32]. Following the definition of the Axiovision software, the average feret ratio was determined as the ratio of the maximum and minimum diameter of the microspheres. These values can vary between 0 and 1 [33]. Microspheres with feret ratio close to 1 are accepted as having a good sphericity [34].

The mechanical strength of the sintered microspheres was assessed by side crushing strength (SCS) testing using an Instron 5582 Universal Testing Machine. The strength of a single microsphere loaded between two diametrically opposed contact points was determined. The crushing strength σ_f (Pa) is calculated using the following equation as described by Couroyer et al. [35]:

$$\sigma_f = 2.8 \frac{P_f}{\pi D^2}$$

where P_f (N) is the load at the breaking point and D the diameter (m) of the microsphere. Reported values were calculated as the average crushing strength on a single shaped microsphere (at least 10) prepared under specific conditions with respect to process parameters and suspension compositions.

The cross-section of the sintered microspheres was examined using a cold field emission scanning electron microscope (FEGSEM) of the type Nova Nano SEM 450 (FEI, USA) at 20kV. Thermally treated samples were encapsulated with an epoxy resin and cured at room temperature. Afterwards, the samples were cut and polished in order to analyse the cross-section of the microspheres. The porosity of the microspheres was determined from the cross-sections using the image analysis software ImageJ [36]. The calcium dispersion was detected by a Bruker XFlash Detector 5030 and a Bruker QUANTAX-200 EDS system.

The calcium content in the microspheres was determined by inductively coupled plasma optical emission spectroscopy (ICP-OES analysis, Perkin Elmer, Optima 3000DV) equipped with a cyclonic

spray chamber and a GemCone nebulizer. In order to liberate the calcium ions out of the alumina matrix, a destruction at high temperature was performed. For this acid digestion of the sample, 0.1 to 0.2 g of the test portion was weighed and transferred into a PTFE digestion vessel (DAB-3, Berghof, Germany). Subsequently, 7 ml of hydrochloric acid 32-35 % (Optima Fisher Chemicals) and 3.5 ml of ultrapure water were added. The digestion was performed using a high-pressure PTFE digestion bomb, consisting of a PTFE inner vessel and an outer stainless steel pressure jacket. The digestion was performed in a heating block (DAH-904 Berghof, Germany). The microspheres were heated to 250 °C in 180 minutes and were held at this temperature for 720 minutes. After digesting, the content of the high pressure PTFE digestion bomb was transferred quantitatively and diluted to 50 ml with ultrapure water. For the quantification of Ca, the emission line at 317.933 nm was used. The results were corrected by using rhodium as an internal standard.

Thermogravimetric analysis (TGA) was recorded on a STA 449C Jupiter (Netzsch, Germany) and performed in dry air (70 mL/min). The samples were heated from ambient temperature to 1400 °C with a heating rate of 5 °C/min. The TGA equipment was coupled online to an mass spectrometer Omnistar GSD 301 O2 (Pfeiffer Vacuum, Germany).

In order to examine the sintering behaviour of the microspheres, dilatometry analyses are performed. However, direct dilatometry on the microspheres was not possible due to plastic deformation of the microspheres by the push rod during the analysis. Therefore, dry (green) microspheres were crushed and die pressed into pellets. The analysis on pellets allowed the comparison with pellets of pure alumina. Dilatometry measurements were performed on a 402 C dilatometer (Netzsch, Germany) in dry air (60 mL/min). The samples were heated from ambient temperature to 1650 °C with a heating rate of 3 °C/min.

The crystal phases of the alumina microspheres were investigated by X-ray diffraction (XRD) on the powders obtained by milling the microspheres. The XRD spectra were recorded on a PANalytical X'Pert PRO MPD diffractometer with filtered Cu Kα radiation. Measurements were done in the 2Θ

mode using a bracket sample holder with a scanning speed of 0.04 °/4 s continuous mode. Rietveld analysis was applied to identify and quantify the crystal phases.

3. Results and discussion

3.1. Ceramic suspension

First step in the shaping process is the characterization of the alumina-alginate suspension by rheological analysis. Since the suspension exhibits a non-Newtonian flow behaviour, it is necessary to characterize the complete viscosity curves of the different suspensions (Table 1). Figure 2 shows the viscosity curves for the different suspensions as a function of the shear rate. The rheology profile of all of the suspensions exhibit a shear thinning behaviour at increasing shear rates. At high shear rates the agitating action in the suspension breaks down the rigid structure by reducing the particle-particle interaction. This results in a decrease of the viscosity. This shear thinning behaviour is dependent on the powder content of the suspension as shown in Figure 2. Increasing the powder content inhibits the free movement of the particles in the suspension, resulting in increase of viscosity at lower shear rates. Therefore, the shear thinning behaviour is more distinct in suspension 40P/0.88LA. Besides powder content, also alginate concentration and type have an influence on the shear thinning behaviour of the alumina suspension. Increasing the alginate concentration results in a rheological behaviour with a more distinct decrease of viscosity in the shear rate range of the shaping process (20P/1.48LA compared to 20P/0.56LA). Changing the alginate type increased the overall viscosity in the whole measured shear rate range.

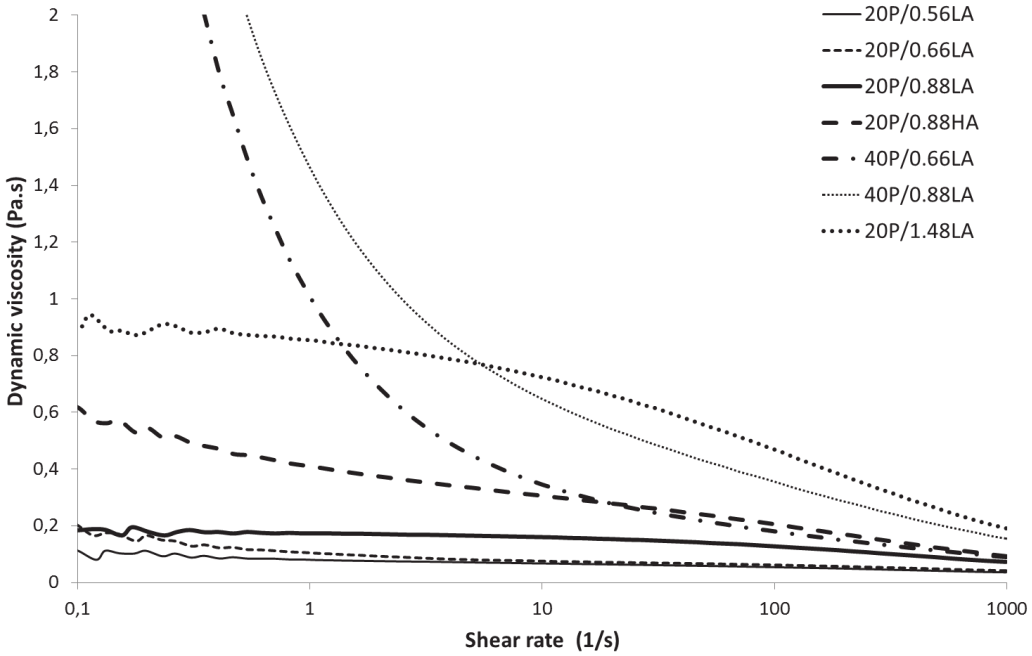

Figure 2: Rheology of the ceramic suspensions

The shear rate at the nozzle depends on the following process parameters and can be estimated by the method described by Martinez et al. [37]. The shear rate $\dot{\gamma}$ is calculated from the superimposed flow rate Q (m^3/s) and the nozzle radius R (m):

$$\dot{\gamma} = \frac{4.\,Q}{\pi.\,R^3}$$

This method enabled the estimation of the working shear rate for each suspension composition at the different nozzles sizes used in this article. The shear rate of the 20P/0.56LA and 20P/1.48 LA suspensions in the used nozzle size ranges varied between 7000 and 360000 s^{-1} (supplementary data figure A). This shear rates exceed the limits of the conventional rheology measurement apparatus. Therefore, the actual viscosity at the nozzle could not be determined.

3.2. Influence of physical parameters on the shaping of microspheres

The key point of controlled shaping of microspheres by vibrating nozzle technology is a jet break-up of the suspension. A stable shaping process is determined by a uniform size distribution of the droplets, uniform distance between the droplets and no disturbing movement of the droplets in the

flow. The vibrational droplet coagulation technology is physically controlled by the frequency and amplitude of the vibration and the feed pressure on the suspension. Moreover, the nozzle diameter dictates the prior parameters. Sakai et al. [38] reported the influence of frequency, amplitude and liquid velocity on jet break-up of Newtonian liquids. Later, the same effects were reported by Heinzen et al. [11] on the jet break-up of pure alginate solutions. The current work correlates the physical parameters and the jet break-up to the shaping process making use of a powder loaded alginate suspension. Although reported differently in literature [38], experiments have shown minimal impact in varying the amplitude at constant nozzle size. Therefore, in this study, the amplitude was kept constant at a value of 1500 mV for the all the experiments at nozzle size 500µm. When the nozzle size is changed, the amplitude does play a role. Decreasing the nozzle size implies an increase in amplitude (up to 3000 mV) following the same trend as the frequency.

3.2.1. Influence of nozzle diameter

One of the parameters influencing droplet generation is the nozzle diameter. These diameters varied in this research between 100 and 1000 µm. Suspensions rheology plays a restrictive role in the choice of the nozzle sizes [27]. Therefore, the influence of the nozzle size is investigated using two suspensions with different viscosity behaviours. Both suspensions contain the same amount of Al_2O_3 powder (20 wt%) but different alginate concentrations, 0.56 wt% (sample 20P/0.56LA) and 1.48 wt% (sample 20P/1.48LA), respectively. The linear relation between the nozzle diameter and the average microsphere size is illustrated in Figure 3. High suspension viscosity (20P/1.48LA) involved a size range between 530 and 1160 µm, since the nozzle size range was limited between 300 and 1000 µm. Shaping microspheres using small nozzles , e. g. with sizes between 100 and 200 µm, was not possible as the highest pressure limit (1000mbar) was inadequate to obtain a stable laminar flow for this high viscosity suspension. This could be overcome by decreasing the alginate content in the suspension, causing a lower viscosity, which enabled the shaping of microspheres through a 100 and 200 µm nozzle. As such, dry microspheres with sizes between 150 and 900 µm are obtained. Additionally, the corresponding feret ratio of these microspheres is shown in Figure 3. The feret ratio

indicates the sphericity of the microspheres and it should be noted that the smaller microspheres (100 and 200 µm) obtained using the 20P/0.56LA suspension seem to have a slightly lower feret ratio. This can be explained by the higher frequencies needed to break-up the jet, causing the droplets to fall in the coagulation bath with less distance between them. The smaller the distance, the more chance to obtain two attached microspheres (twins). Since twins have typically an elongated shape, smaller feret ratios are obtained. The resulting data indicated that low viscosity suspension is better suited to obtain small microspheres while higher suspension viscosity is better suited for larger microspheres formation.

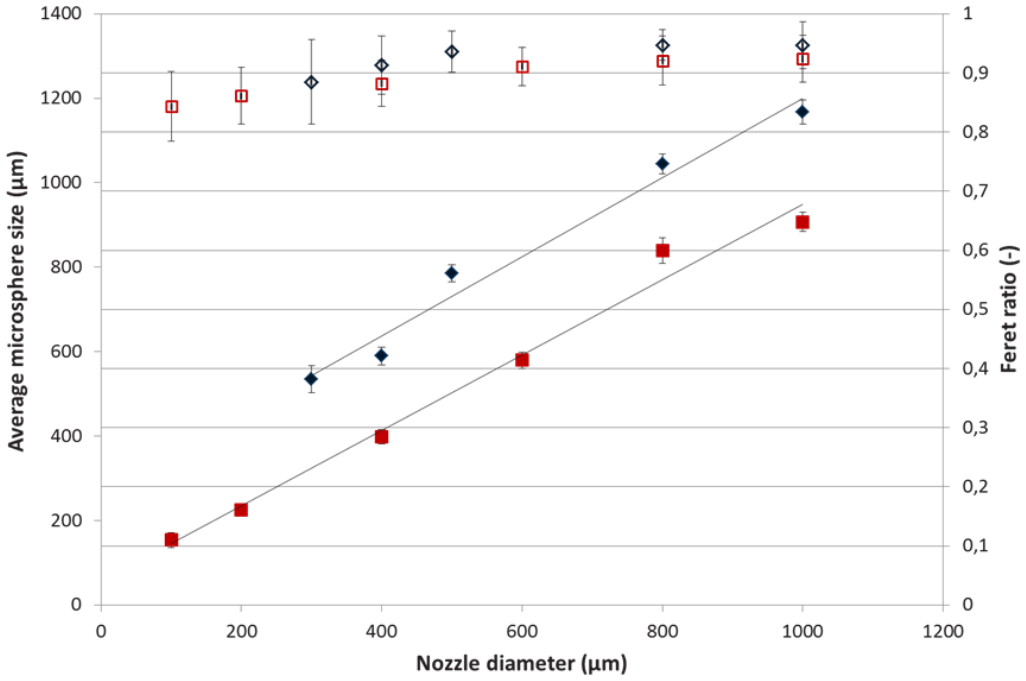

Figure 3: Influence of nozzle diameter on average dry microsphere size (filled bullets) and the feret ratio (open bullets) for two different ceramic suspensions: 20P/0.56LA (red square) and 20P/1.48LA (blue diamond).

3.2.2. Influence of process variables

In conjunction with the nozzle diameter, it is possible to modify the shaping process by varying the pressure and frequency.

Figure 4 depicts the influence of these process variables on the average size of the wet microspheres. The results are obtained from the wet microspheres, to avoid the effects of the drying behaviours of

the different suspensions. Four different suspensions (Table 1) were shaped with a 500 µm nozzle at different frequencies and pressures that allowed a stable jet break-up. All four suspensions had a specific stable pressure and frequency range, dependent on their viscosity, visible as the range in which data points are collected. For example, starting with the 20P/0.88HA suspension a range of 320-370 mbar at a constant frequency of 300 Hz was applied. In addition, it was possible to vary the frequency between 185-330 Hz at a constant pressure of 350 mbar.

Two correlations between the average size of the wet microspheres and the process variables, pressure and frequency, are found.

The first correlation is visible on the pressure results. Figure 4A shows the influence of the applied pressure (and thus the flow of the suspension) on the average size of the microspheres for the four suspensions. Pressure differences can be applied to change the microsphere dimensions but the absolute range is always dictated by the composition of the suspension. It is clear that the average microsphere size increases with increasing pressure in each suspension applied. Furthermore, increasing the suspensions viscosity necessitates an increase of pressure on the feed tank. By increasing the pressure, the microspheres also enlarged due to the increased amount of suspension in a droplet of the liquid jet. The viscosity of the suspensions is compared at a shear rate of 1000 s^{-1} and assuming linear behaviour above this shear rate: 20P/0.88LA > 20P/0.88HA > 40P/0.66LA > 20P/1.48LA. A specific case is the sample 20P/1.48LA. As seen in Figure 2, the viscosity of this suspension is nearly four times as high as the viscosity of 20/0.88LA. This required a higher pressure to induce a good jet break-up, resulting in larger microspheres.

The second correlation between average size and process variables was established by changing the frequency at a constant pressure of 350 mbar in (Figure 4B). Contrary to the pressure, a decrease in microsphere size is observed when the frequency of the vibration was increased within each suspension. This decrease in microsphere size is due to the concept of the jet break-up. Each vibration at a certain frequency represents a droplet. When pressure is kept constant, the same

amount of suspension is flowing through the nozzle and breaks into smaller droplets as a result of the increased frequency. Small influences of the suspension's viscosity were observed on the frequency process window. Low viscosity (20P/0.88LA) required higher frequencies to obtain a stable jet break-up. The three other suspensions with a higher viscosity all showed a stable jet break-up in the same frequency range. When looking at the size ranges for each suspension obtained by varying pressure or frequency, it is clear that changing frequency allows a much larger size range within one type of suspension.

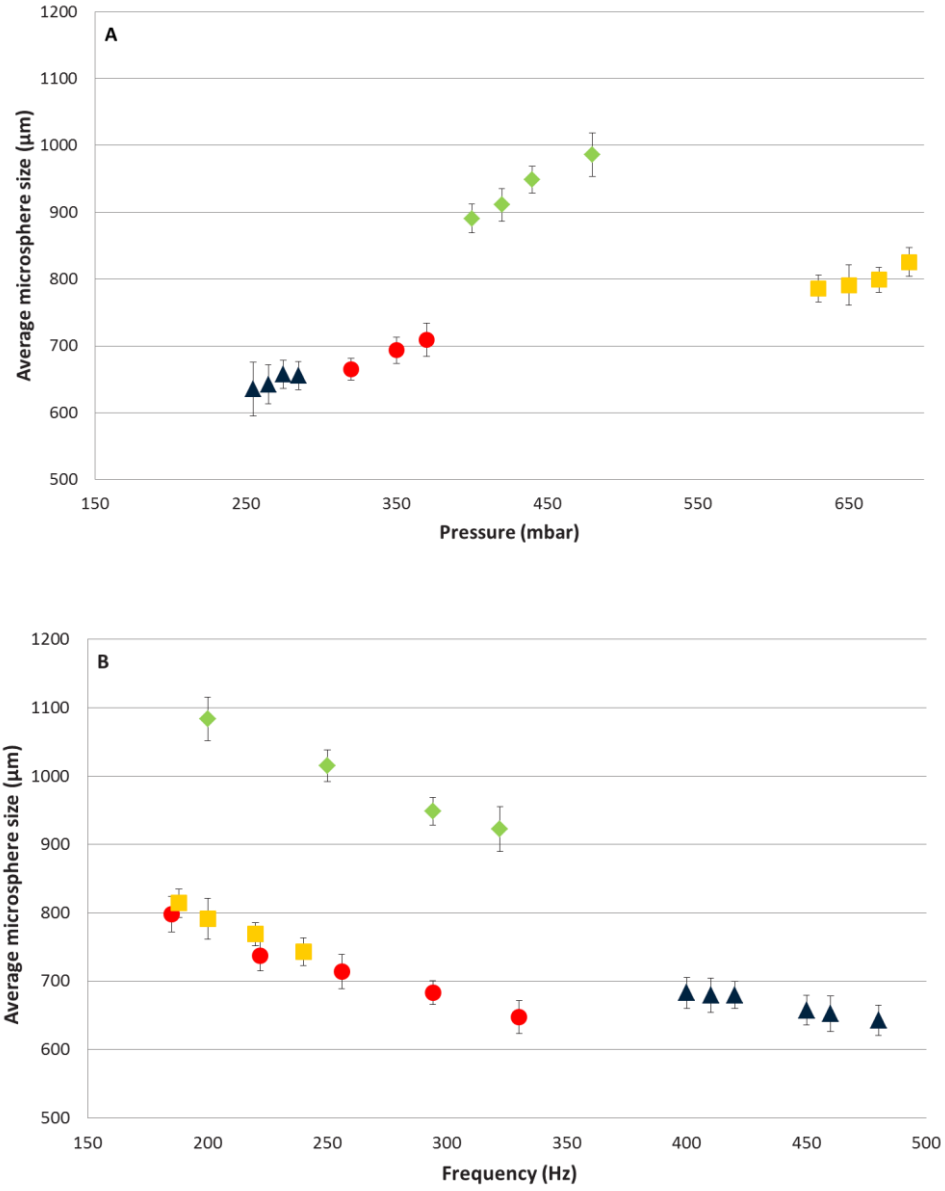

Figure 4: Influence of process variables on the shaping of wet alumina microspheres using different ceramic suspensions and a 500 µm nozzle at A: constant frequency of 300 Hz and B: constant pressure of 350 mbar. 40P/0.66LA (green diamond), 20P/1.48HA (yellow square), 20P/0.88HA (red dot), 20P/0.88LA (blue triangle).

However, when taking into account all three parameters: frequency, pressure and suspension composition, a much wider range of microsphere sizes can be designed applying the same nozzle size. Changing the average microsphere size by varying the pressure and frequency had no impact on the sphericity of the microspheres. (Supplementary Figure B) Therefore, a stable process window for shaping alumina microspheres with constant nozzle size was established. This allows a wide control of the average microsphere size by tuning the suspension and process variables. In this case wet microspheres are shaped in a size range between 900 and 1400 µm with a nozzle of 500 µm.

3.3. Post processing of alumina microspheres

After shaping the microspheres, another crucial step in obtaining alumina microspheres is the thermal post processing step to remove the organic matter and produce dense alumina microspheres. The impact of the post processing will be explained on the 20P/1.48LA microspheres, shaped with a single nozzle with an inner diameter of 500 µm.

3.3.1. Calcination

In order to control and understand the calcination of the calcium alginate in the alumina microspheres, several thermal analyses were performed. By performing the thermogravimetric analysis coupled with a mass spectrometer (TGA-MS), the calcination process was simulated showing weight losses at several temperature intervals and their corresponding calcination products as a function of the heating temperature. The weight loss and derivative of the weight loss profiles (TG/DTG) and MS data are shown in Figure 5 and Figure 6.

The TG/DTG profiles show a first weight loss in the temperature range of 30 to 200 °C with a DTG maximum at 95°C corresponding to the evolution of H_2O (m/z=18) in the MS data (Figure 6). This may be attributed to the desorption of physically absorbed water and removal of structural water (dehydration reactions). The oxidation of the calcium alginate occurs in a two-step process with DTG maxima at 245 °C and 375 °C and is confirmed with the detection of H_2O and CO_2 (m/z=44) starting at 175 °C [39]. Parallel to the oxidation of the calcium alginate, the concomitant formation of crystalline $CaCO_3$, calcite is identified in the ex-situ XRD analysis (Figure 7). As visible in these XRD analysis, the calcite formation occurred at temperatures above 300 °C. Further, the DTG profile indicates weight losses between 400 and 600°C which could be attributed to a decarboxylation reaction, since only CO_2 is visible in the mass spectra. Based on the ex-situ XRD analysis, the decomposition of $CaCO_3$ occurred above 600°C, but no CO_2 signal was reported in the mass spectra. Since the decomposition occurs in a broad temperature range, low concentrations of CO_2 were released per temperature unit, resulting in signals below the detection limit of the mass spectrometer. Signals of $CaCO_3$ remained

visible up to 1000°C on the ex-situ XRD analysis. The detailed mechanism of the solid state reaction between $CaCO_3$ and Al_2O_3 in function of temperature are described in detail later in the section 3.3.2.

Based on the TGA-MS data, a calcination step of 1 hour at 600 °C was introduced in the thermal post treatment of the microspheres.

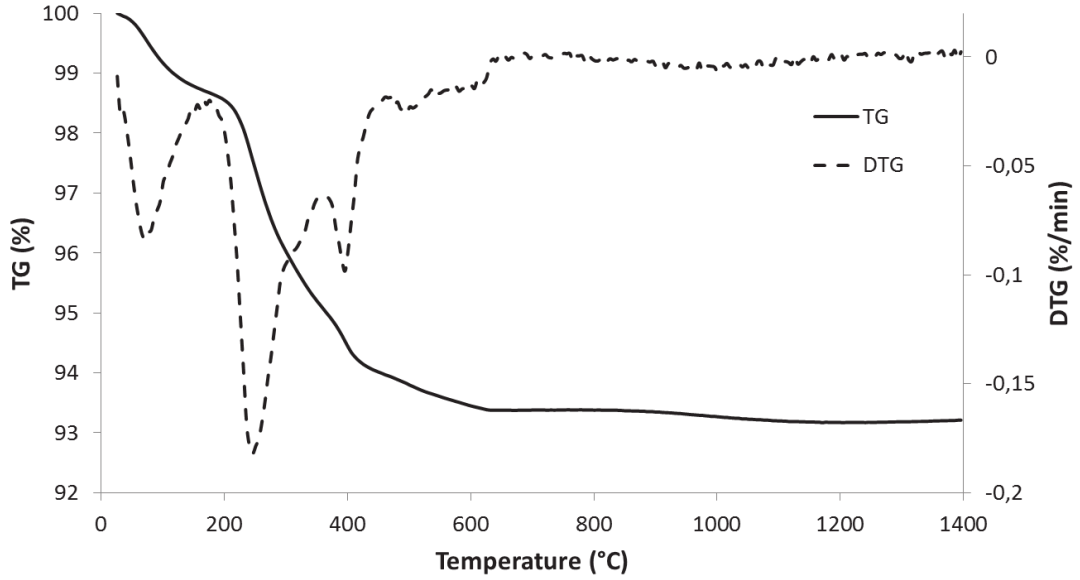

Figure 5: TG and DTG of the 20P/1.48LA microspheres in function of temperature under air flow

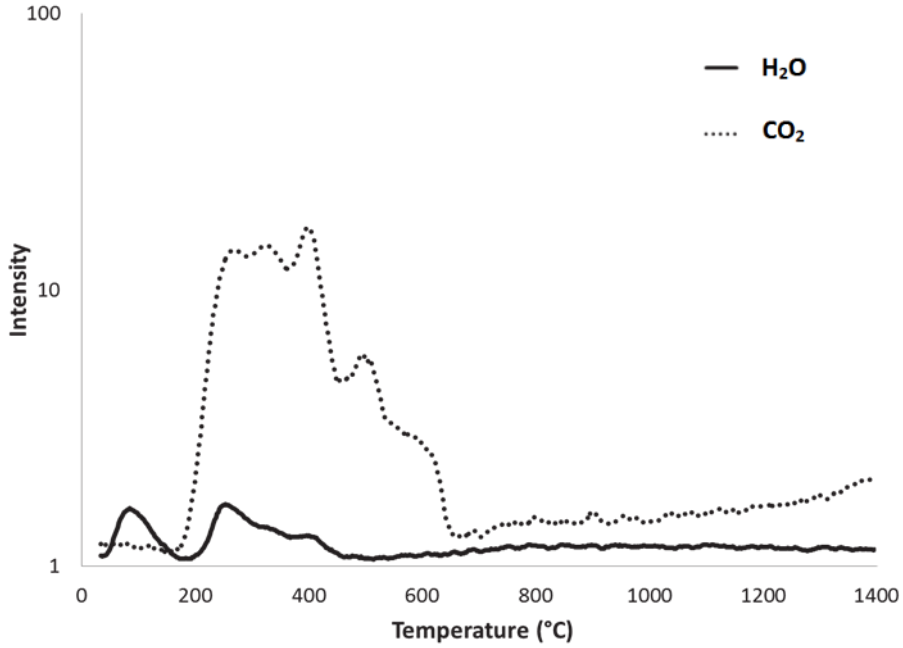

Figure 6: Mass spectra of the gaseous components evolving during TGA of 20P/1.48LA microspheres in function of temperature

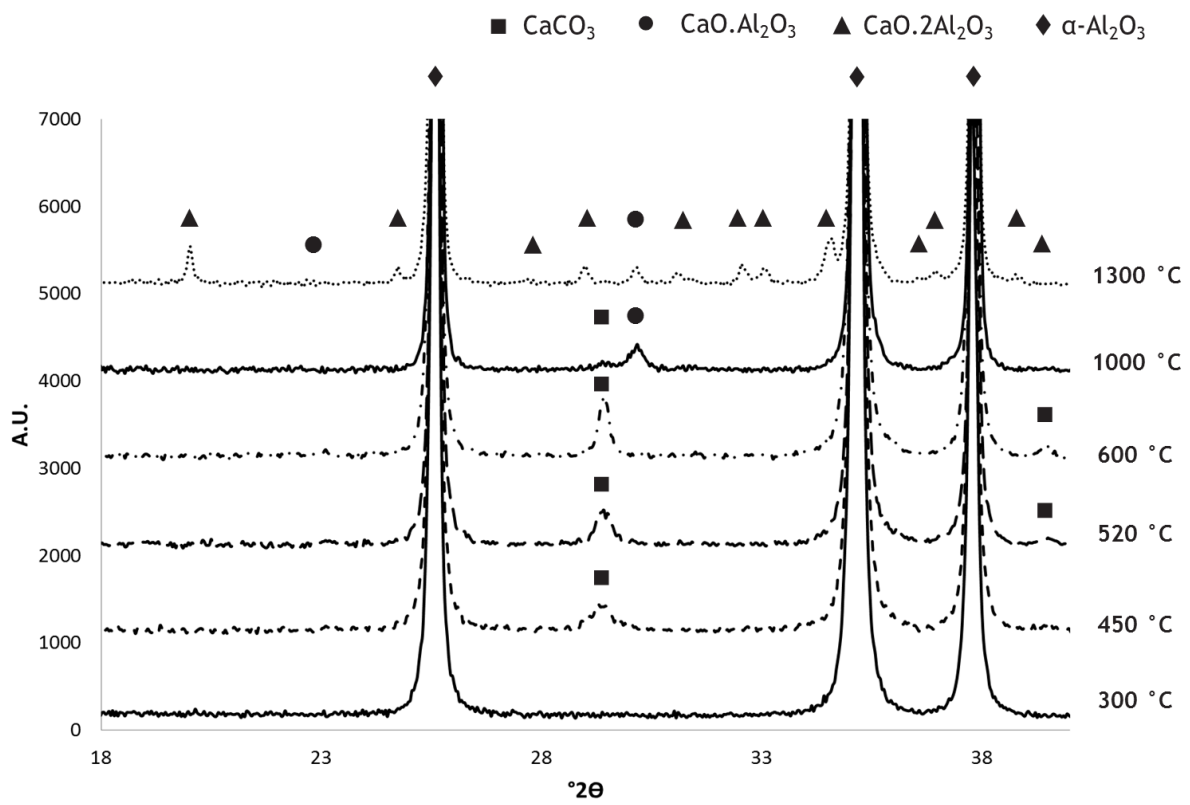

Figure 7: Ex-situ XRD of the calcium alginate calcination in the 20P/1.48LA microspheres at discrete temperature intervals selected based on the TGA weight losses and MS data

3.3.2. Sinter effects

According to the specifications of the pure α-Al_2O_3 powder (SG16), a sintering step of 1 hour at 1540 °C was required in order to complete full densification[40]. Therefore, these conditions were used as a starting point for sintering the alumina microspheres obtained in the present study.

The SEM analysis on the cross section of sintered microspheres by using this sinter profile (Figure 8A), revealed 14% of porosity. In order to obtain full densification of the microspheres, a higher sinter temperature (1650 °C) was used for further sinter tests as suggested by Santos et al [13]. The total porosity decreased to 1.5 % and pore sizes enlarged due to the merging of small pores in the densification process as observed in Figure 8B.

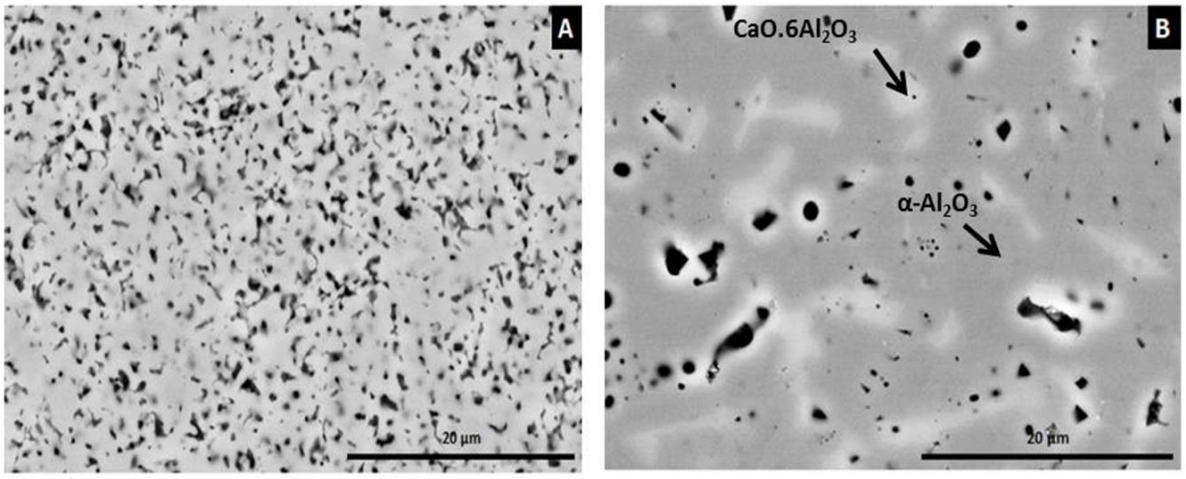

Figure 8: SEM images of the cross sections of the 20P/1.48LA Al_2O_3 microspheres sintered at 1540 °C (A) and 1650 °C (B)

Besides the decreased porosity, the SEM images reveal the presence of an extra crystal phase (the lighter parts in Figure 8B) in the α-Al_2O_3 matrix. This extra crystal phase can be correlated with the presence of calcium forming an extra phase in the calcination and sintering process, respectively. As suggested in the ex-situ XRD, $CaCO_3$ is present after the calcination of calcium alginate. A solid state reaction between $CaCO_3$ and α-Al_2O_3 leads to the formation of a calcium hexaluminate phase, $CaO.6Al_2O_3$, as illustrated by the following suggested reaction sequence between $CaCO_3$ and Al_2O_3 described in literature [41][42]:

$$CaCO_3 + Al_2O_3 \rightarrow CaO + Al_2O_3 + CO_{2\,(gas)} \quad (1)$$

$$CaO + Al_2O_3 \rightarrow CaO.Al_2O_3 \quad (2)$$

$$CaO.Al_2O_3 + Al_2O_3 \rightarrow CaO.\,2Al_2O_3 \quad (3)$$

$$CaO.2Al_2O_3 + 4Al_2O_3 \rightarrow CaO.6Al_2O_3 \quad (4)$$

Several stable calcium aluminate phases could be formed in the reaction sintering of Al_2O_3 microspheres shaped with alginate. As indicated by the ex-situ XRD analysis (Figure 7), the evolution of calcium aluminate phases is driven by increased temperatures. Starting at 1000 °C the first intermediate product ($CaO.Al_2O_3$) becomes visible in the X-ray diffractogram, next to the residue

$CaCO_3$ of the calcination process. XRD analysis on the sample heat treated at 1300°C shows a combination of both $CaO.Al_2O_3$ and $CaO.2Al_2O_3$ in the α-Al_2O_3 matrix and no more $CaCO_3$ is detected. The $CaO.Al_2O_3$ and $CaO.2Al_2O_3$ phases reacted both in $CaO.6Al_2O_3$ when sintering the microspheres at 1650°C. This is visible in the XRD analysis in Figure 9. The combination of α-Al_2O_3 and $CaO.6Al_2O_3$ at 1650°C is in correlation with the phase diagram of Al_2O_3/CaO [43]. Tungsten carbide (TC) originates from the sample preparation of the XRD analysis.

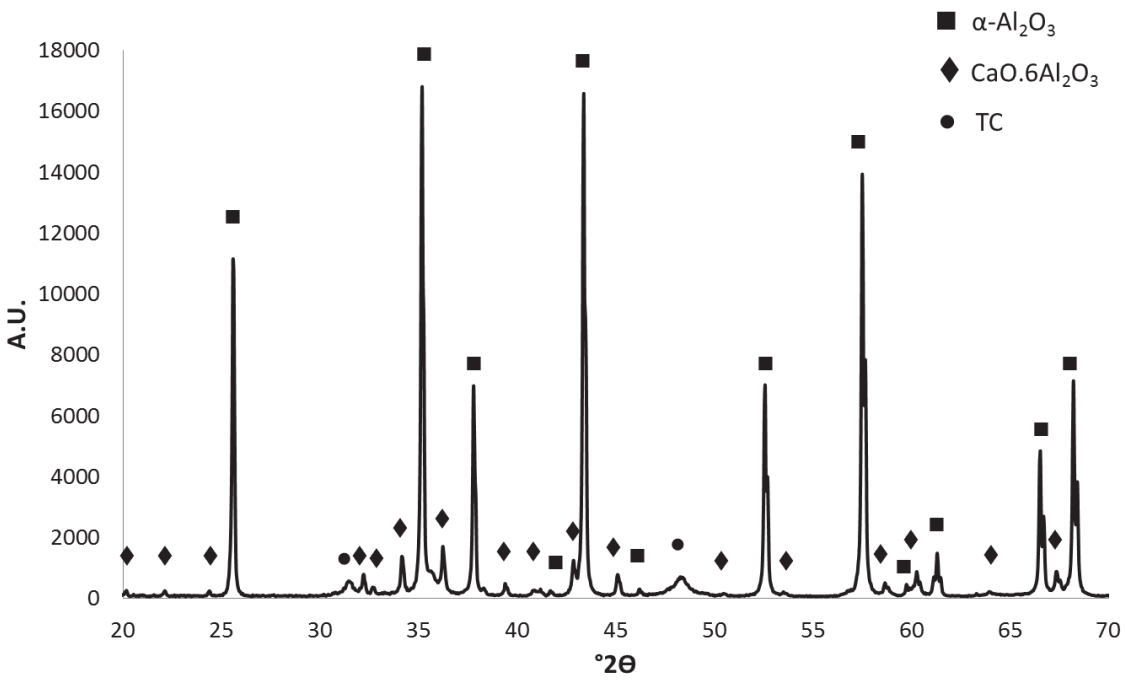

Figure 9: XRD analysis of 20P/1.48LA microspheres sintered 1h at 1650 °C

Several factors should be considered when studying the grain growth and orientation of the $CaO.6Al_2O_3$ phase, such as the calcium content and the pore size and distribution, respectively. It is well known that calcium as a dopant in α-Al_2O_3 materials causes elongated grain growth in the sintering process [44][45]. As it was previously reported by Dominguez et al. [41], larger pore sizes in the calcined material promotes the formation of elongated grains of $CaO.6Al_2O_3$. The smaller the pore sizes in the material, the more grain boundaries are formed around the α-Al_2O_3 grains, which further inhibit the grain growth of the hexaluminate. Figure 10 represents SEM-EDX analysis on the cross section of the 20P/1.48LA microspheres after sintering at 1650 °C. It can be seen that the

calcium is spread homogenously in the microspheres, leading to a homogenous network of the calcium hexaluminate. No distinct correlation between the $CaO.6Al_2O_3$ presence and porosity was found in the cross section of the microspheres.

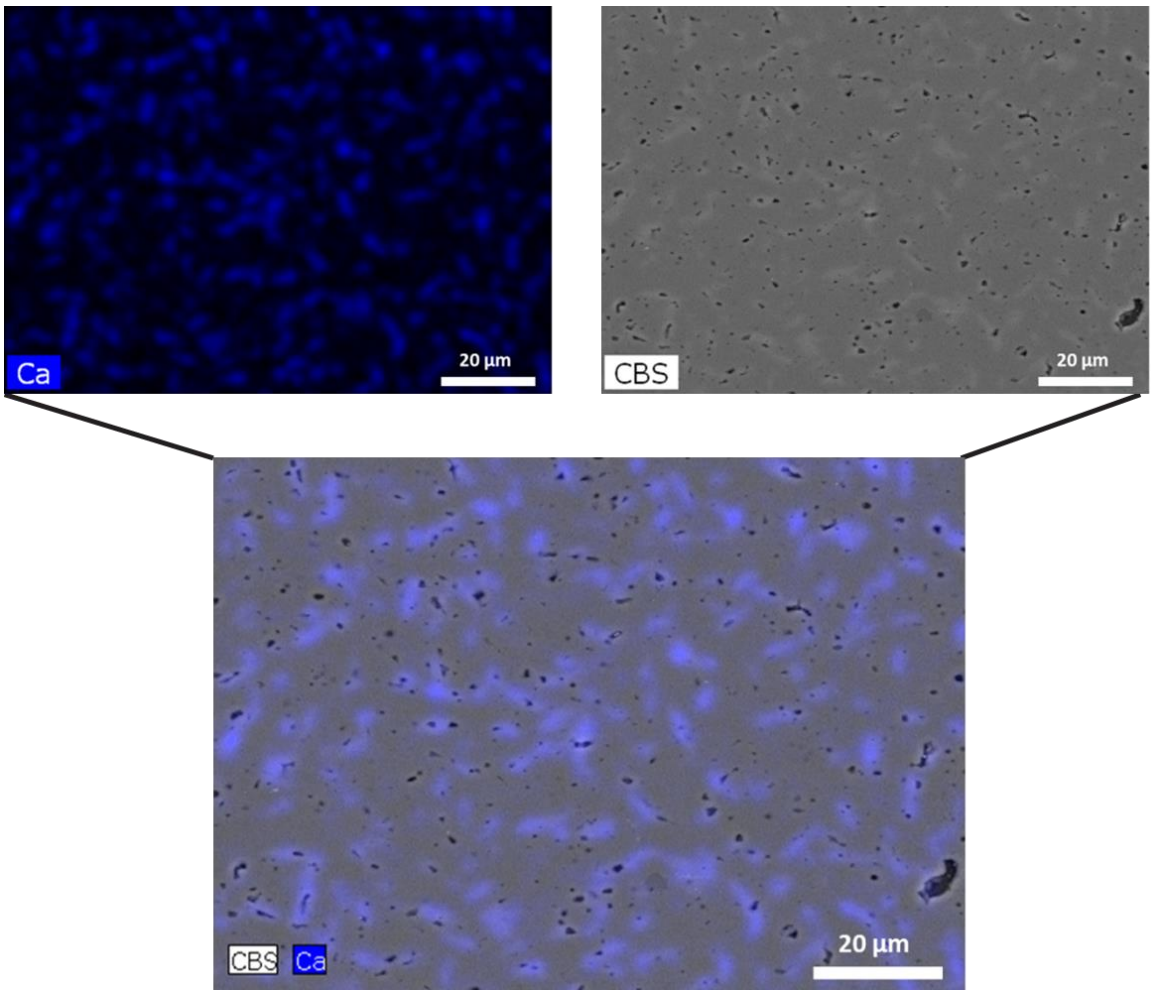

Figure 10: SEM-EDX analysis of calcium presence and porosity in 20P/1.48LA microspheres sintered at 1650 °C.

Besides the influence on the microstructure, a second effect of the calcium on the sintering occurs. Dilatometry results are represented in Figure 11. When compared to pure alumina, which started to densify at 1032 °C, the presence of the calcium aluminate phases raised the onset temperature to 1265 °C for the 20P/1.48LA sample. Dilatometry analyses on the microspheres with different compositions are represented in Supplementary Figure D. It is shown that all onset temperatures increased compared to the pure Al_2O_3 pellet. Onset temperatures of the samples with a constant powder content increased in relation with the increased calcium content (Table 2): pure Al_2O_3 <

20P/0.88LA-20P/0.88HA < 20P/1.48LA. This relation designates that the formation of $CaO.6Al_2O_3$ hindered the sintering of the samples. This effect is in correlation with previous work done on the sintering of $Al_2O_3/CaO.6Al_2O_3$ composite materials [46]. Sample 40P/0.66LA does not follow the relation as described above, which could be correlated to the higher powder content resulting in a different calcium distribution in the sample.

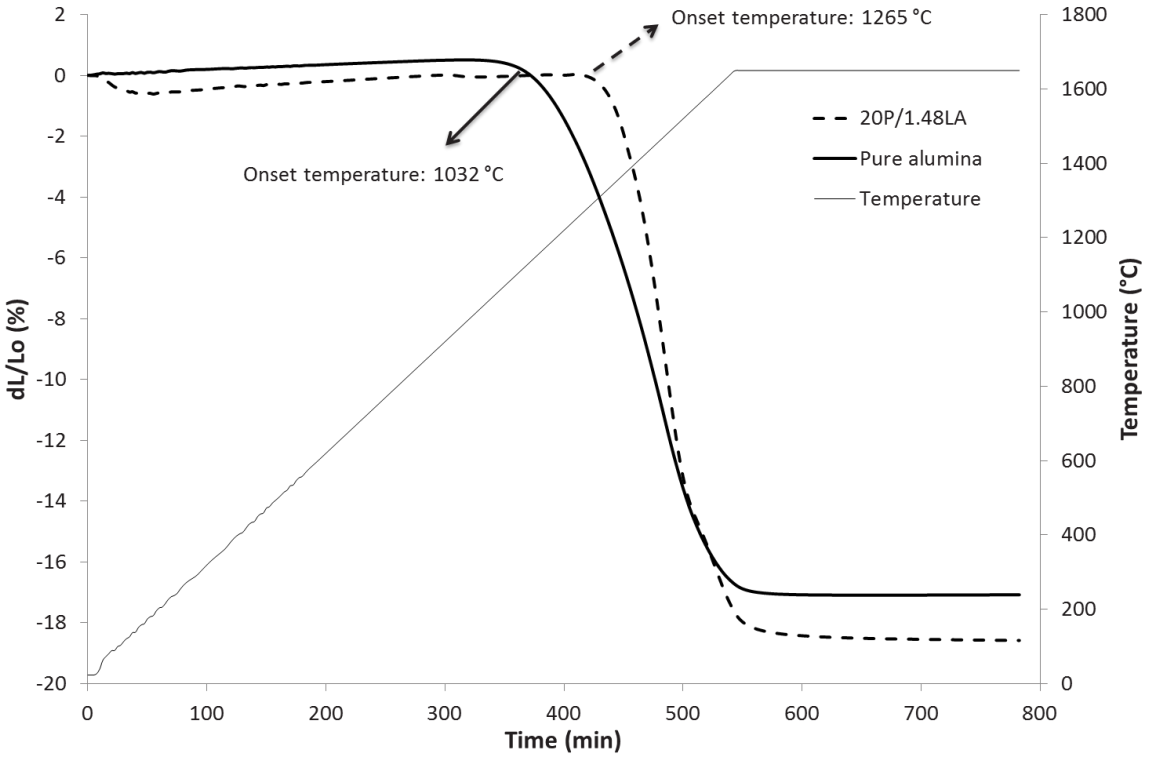

Figure 11: Dilatometry analysis on pellets of pure alumina and 20P/1.48LA microspheres

3.3.3. Shrinkage behaviour

In the interest of controlling the entire shaping process of alumina microspheres, shrinkage of the wet microspheres during drying and sintering was examined. Shrinkage was homogeneous in all directions of the microspheres, resulting in dried microspheres with a similar feret ratio as the wet microspheres (Supplementary Figure C). By following the shrinkage throughout the whole process, it is possible to predict the resulting sintered microsphere size for a constant suspension composition (Figure 12). The shrinkage from wet to dry microspheres is controlled by the evaporation of the water inside the microspheres. In order to promote this process, the water was replaced by isopropyl

alcohol in the washing step. This resulted in a decrease of capillary forces in the microsphere, retaining the spherical shape during drying.

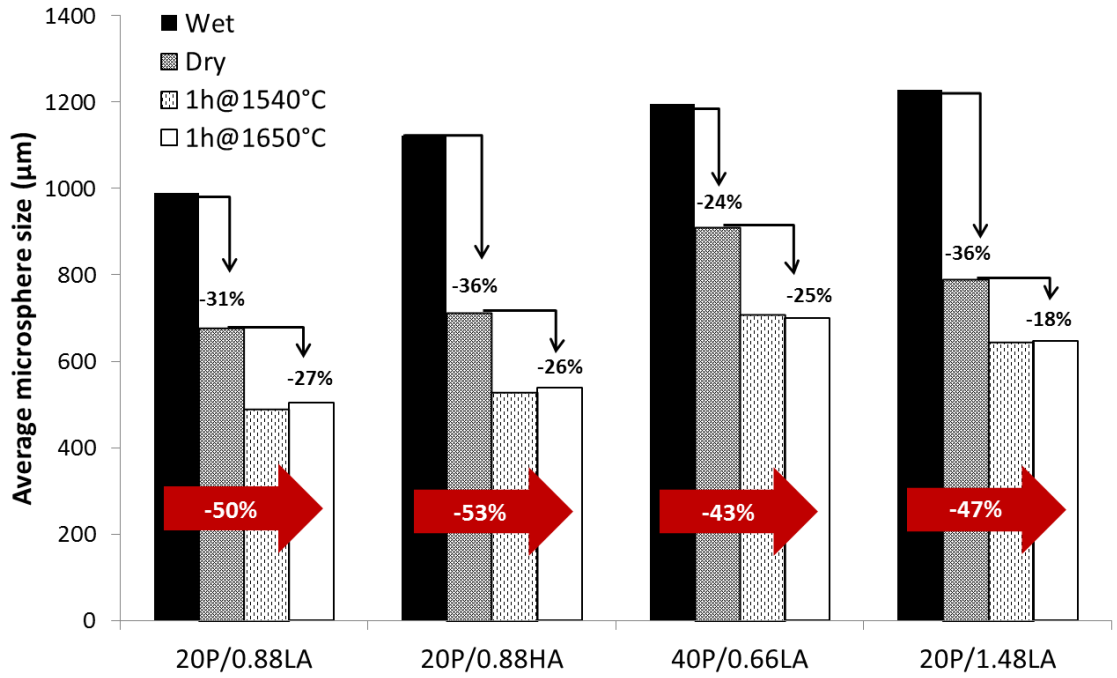

Figure 12: Shrinkage overview of the different alumina microspheres over the various post processing steps

It can be observed (Figure 12) that the shrinkage degree from wet to dry microspheres is larger when using a higher concentration of alginate (20P/1.48LA) or an alginate with a higher viscosity (20P/0.88HA). When looking at total shrinkage behaviour, as expected, a lower shrinkage degree (-43 %) was visible when the powder loading was doubled in the feed suspension (40P/0.66LA). This is mainly due to a diminished shrinking upon drying. In addition, less sinter shrinkage was noticed when sintering the 20P/1.48LA microspheres. This difference may be well correlated with the reactive sintering into the $CaO.6Al_2O_3$ phase, which is characterized by a lower density (3.79 g/cm³) in comparison with the α-Al_2O_3 phase (3.89 g/cm³). As the 20/1.48LA sample has a double amount of $CaO.6Al_2O_3$ in its structure (Table 2), this might be responsible for the difference in sinter shrinkage.

3.4. Material characteristics

Table 2: Overview of material characteristics of the alumina microspheres, sintered 1h at 1650 °C

	Average microsphere size (µm)	Ca^{2+} mg/kg dry weight	wt% $CaO.6Al_2O_3$ (Calculated)	Wt% $CaO.6Al_2O_3$ (Rietveld)	Compressive strength (MPa)	Porosity (%)
20P/0.88LA	505 ± 10	4260	7	7	456 ± 108	2.0 ± 0.1
20P/0.88HA	538 ± 10	4350	7	7	396 ± 144	1.9 ± 0.4
40P/0.66LA	700 ± 16	1900	3	3	470 ± 75	1.7 ± 0.3
20P/1.48LA	646 ± 7	8430	14	13	810 ± 177	1.5 ± 0.1

The overview of the material characteristics (Table 2) shows the different amounts of Ca^{2+} (analysed by ICP-OES) present in the microspheres after sintering. These differences are correlated to the variation of alginate content in the feed suspension and in accordance to the weight losses in the thermal post processing (Supplementary data Figure E). In the present experimental conditions, a low amount of sodium alginate in the ceramic suspension leads to the presence of less calcium ions in the resulting microspheres. The calcium content may be correlated with the $CaO.6Al_2O_3$ crystal phase allowing the quantification of this additional phase. Assuming that all the calcium present in the matrix is incorporated in the $CaO.6Al_2O_3$ phase during the solid state reaction in the sintering step, the theoretical amounts of the $CaO.6Al_2O_3$ phase can be calculated (see Table 2). Moreover, to verify if calcium could be present in other phases, the wt% of $CaO.6Al_2O_3$ was quantified by XRD analysis using the Rietveld analysis method. When comparing these results, it is shown that the stoichiometric calculation can be correlated to the measured amount in the low calcium containing sample (20P/0.88LA sample), while a small difference can be observed in the 20P/1.48LA sample. In this case it seems as if not all the calcium has been incorporated in the $CaO.6Al_2O_3$ crystal phase.

Since the calcium content is in relation to the initial alginate content it is possible to tune the amount of $CaO.6Al_2O_3$ crystal phase in the obtained microspheres by manipulating the initial suspension composition.

Table 2 gives an overview of the compressive strength of the microspheres and the resulting porosity after sintering as determined by SEM on the cross-section. No large changes in resulting porosity were visible when the alginate and alumina content were varied. The SEM analysis on the surface of the alumina microspheres after sintering at 1650 °C (Figure 13 and Supplementary Figure F) revealed the presence needle-like grains in the microspheres. According to the previous work of Santos et al. [13] the higher compressive strength of the microspheres could be due to this needle-like shape. Further work on these effects is beyond the scope of this article.

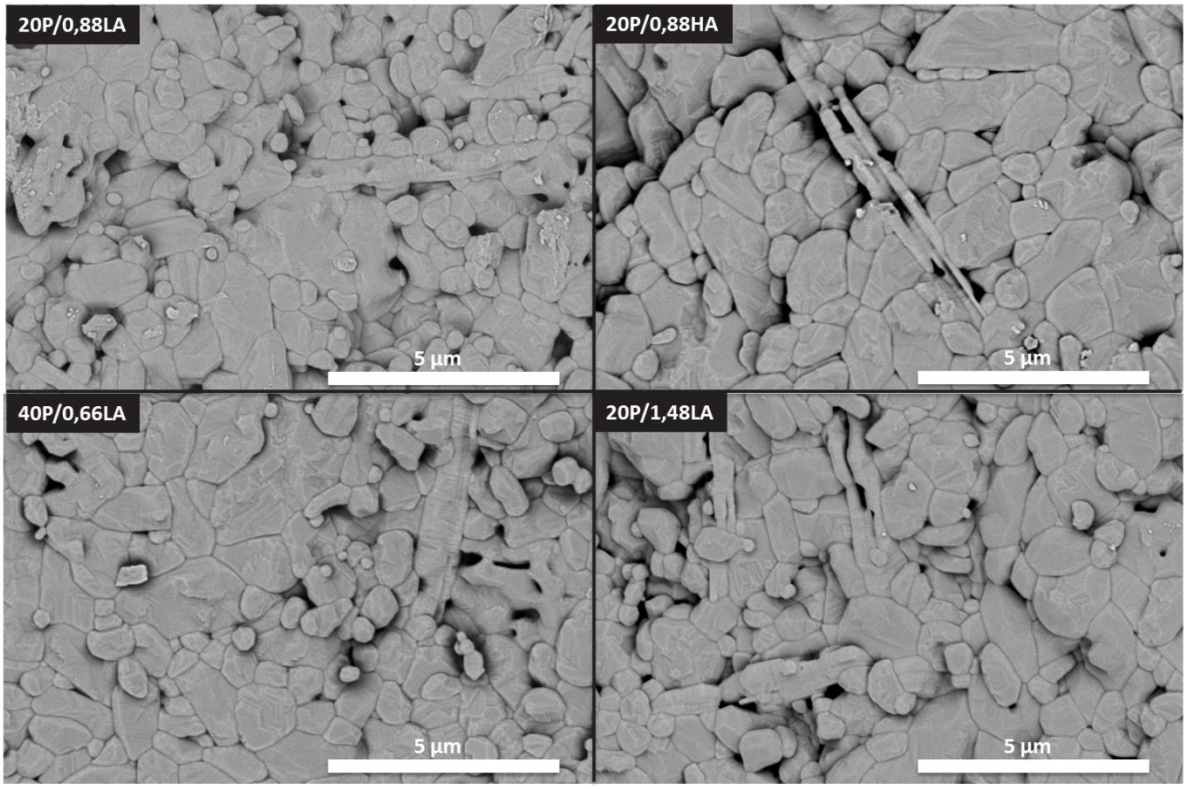

Figure 13: SEM analysis of the outer surface of sintered (1h at 1650 °C) Al_2O_3 microspheres. A: 20P/0.88LA B: 20P/0.88HA C: 40P/0.66LA D:20P/1.48LA

4. Conclusions

The vibrational droplet coagulation system proved to be a successful method to produce alumina microspheres with a uniform size distribution and shape, making use of a sodium alginate loaded alumina suspension. The combination of both physical as well as chemical parameters provides a flexible process and broad window of control and regulate the size of the microspheres while retaining a uniform shape. By changing the powder content, alginate type and concentration, it was possible to tune the viscosity, which further allowed the production of wet microspheres in the range of 900 to 1400 µm by using only a 500 µm nozzle. This was enabled by varying the pressure and/or frequency between the borders of the stable area and/or changing the suspension formulation. The results obtained on the 500 µm nozzle, can be transferred generically to different nozzle sizes, expanding the limits of the current model system. In this way, it is possible to tune the process parameters, in order to meet the requirements of the different applications.

Moreover, the obtained alumina microspheres were characterized by the combination of several techniques, such as TGA-MS, ex situ XRD, SEM and ICP-OES to further elucidate both microstructural characteristics and phase transformations during calcination and sintering post processing steps. As indicated by the TGA-MS data, a $CaCO_3$ phase was present in the calcination process leading to CaO at elevated temperatures, which in combination with α-Al_2O_3 led to the formation of an extra crystal phase with elongated grain distribution (calcium hexaluminate $CaO.6Al_2O_3$) in the sintered materials. The amount of sodium alginate in the feed suspension controlled the calcium concentration in the sintered microspheres. Therefore, it was possible to tune the microstructure and amount of $CaO.6Al_2O_3$ in the end material by tuning the alginate content. Shaping dense alumina microspheres is only the first step in the development of a controlled granulation technique to obtain alumina microspheres. The vibrational droplet coagulation technique can be much more flexible in its ability to make ceramic microspheres as it can be adapted to obtain microspheres with varying sizes, porosity and microstructure.

Acknowledgment

This work was supported the Agency for Innovation by Science and Technology in Flanders (IWT-131229) which granted J. Pype her PhD scholarship. E. M. Seftel greatly acknowledges the Fund for Scientific Research – Flanders (FWO – Vlaanderen) for financial support. The authors gratefully acknowledge the technical assistance of the VITO personnel (Unit Sustainable Materials management), especially A. De Wilde (TGA-MS), M. Mertens (XRD), R. Kemps and D. Vanhoyweghen (SEM). In addition they thank Filip Beutels (VITO) for the ICP-OES measurements.

References

[1] A. Agrawal, A. Satapathy, Thermal and dielectric behaviour of polypropylene composites reinforced with ceramic fillers, J. Mater. Sci. Mater. Electron. 26 (2015) 103–112. doi:10.1007/s10854-014-2370-8.

[2] M. Ohashi, S. Kawakami, Y. Yokogawa, G.C. Lai, Spherical aluminum nitride fillers for heat-conducting plastic packages, J. Am. Ceram. Soc. 88 (2005) 2615–2618. doi:10.1111/j.1551-2916.2005.00456.x.

[3] S. Aguado, J. Canivet, D. Farrusseng, Facile shaping of an imidazolate-based MOF on ceramic beads for adsorption and catalytic applications, Chem. Commun. 46 (2010) 7999. doi:10.1039/c0cc02045a.

[4] D.L. Trimm, H. Arai, M. Machida, Thermal stabilization of catalyst supports and their application to high-temperature catalytic combustion, Appl. Catal. A Gen. 138 (1996) 161–176. doi:10.1016/0926-860X(95)00294-4.

[5] Z.R. Ismagilov, R.A. Shkrabina, N.A. Koryabkina, New technology for production of spherical alumina supports for fluidized bed combustion, Catal. Today. 47 (1999) 51–71. doi:10.1016/S0920-5861(98)00283-1.

[6] T.Y. Klein, L. Treccani, K. Rezwan, Ceramic Microbeads as Adsorbents for Purification Technologies with high specific surface area, adjustable pore size and morphology obtained by ionotropic gelation, J. Am. Ceram. Soc. 95 (2012) 907–914.

[7] A.B.D. Nandiyanto, K. Okuyama, Progress in developing spray-drying methods for the production of controlled morphology particles: From the nanometer to submicrometer size ranges, Adv. Powder Technol. 22 (2011) 1–19. doi:10.1016/j.apt.2010.09.011.

[8] B.-B. Lee, P. Ravindra, E.-S. Chan, Size and Shape of Calcium Alginate Beads Produced by Extrusion Dripping, Chem. Eng. Technol. (2013) 1627–1642. doi:10.1002/ceat.201300230.

[9] C.G. De Kruif, F. Weinbreck, R. De Vries, Complex coacervation of proteins and anionic polysaccharides, Curr. Opin. Colloid Interface Sci. 9 (2004) 340–349. doi:10.1016/j.cocis.2004.09.006.

[10] S.K. Karode, S.S. Kulkarni, a. K. Suresh, R. a. Mashelkar, New insights into kinetics and thermodynamics of interfacial polycondensation, Chem. Eng. Sci. 53 (1998) 2649–2663. doi:10.1016/S0009-2509(98)00083-9.

[11] C. Heinzen, A. Berger, I. Marison, Use of Vibration Technology for Jet Break-Up for Encapsulation of Cells and Liquids in Monodisperse Microcapsules, in: Fundam. Cell Immobil. Biotechnol., 2004: pp. 257–275. doi:10.1007/978-94-017-1638-3_14.

[12] M. Whelehan, I.W. Marison, Microencapsulation using vibrating technology, J. Microencapsul. 28 (2011) 669–688. doi:10.3109/02652048.2011.586068.

[13] C.J.E. Santos, T.-S. Wei, B. Cho, W.M. Kriven, A Forming Technique to Produce Spherical Ceramic Beads Using Sodium Alginate as a Precursor Binder Phase, J. Am. Ceram. Soc. 96 (2013) 3379–3388. doi:10.1111/jace.12584.

[14] R.H. Plovnick, Shaped silicon nitride bead aggregates, Mater. Res. Bull. 34 (1999) 2137–2141. doi:10.1017/CBO9781107415324.004.

[15] F. Ferauche, N. Winterton, C. Alié, Characterization of low-density silica xerogel formed into microspheres, J. Non. Cryst. Solids. 352 (2006) 8–17. doi:10.1016/j.jnoncrysol.2005.11.025.

[16] C. Alié, F. Ferauche, B. Heinrichs, R. Pirard, N. Winterton, J.-P. Pirard, Preparation and characterization of xerogel catalyst microspheres, J. Non. Cryst. Solids. 350 (2004) 290–298. doi:10.1016/j.jnoncrysol.2004.05.019.

[17] J. Roosen, J. Pype, K. Binnemans, S. Mullens, Shaping of Alginate–Silica Hybrid Materials into Microspheres through Vibrating-Nozzle Technology and Their Use for the Recovery of Neodymium from Aqueous Solutions, Ind. Eng. Chem. Res. 54 (2015) 12836–12846. doi:10.1021/acs.iecr.5b03494.

[18] A. Haug, O. Smidsrød, B. Larsen, S. Gronowitz, R.A. Hoffman, A. Westerdahl, The Effect of Divalent Metals on the Properties of Alginate Solutions. II. Comparison of Different Metal Ions., Acta Chem. Scand. 19 (1965) 341–351. doi:10.3891/acta.chem.scand.19-0341.

[19] L. Bergström, Shear thinning and shear thickening of concentrated ceramic suspensions, Colloids Surfaces A Physicochem. Eng. Asp. 133 (1998) 151–155. doi:10.1016/S0927-7757(97)00133-7.

[20] Z. Yu, Y. Huang, C. Wang, S. Ouyang, A novel gel tape casting process based on gelation of sodium alginate, Ceram. Int. 30 (2004) 503–507. doi:10.1016/j.ceramint.2003.08.003.

[21] I. Santacruz, C.A. Gutiérrez, M.I. Nieto, R. Moreno, Fast consolidation in aqueous tape casting through alginate gelation, Adv. Eng. Mater. 3 (2001) 906–909. doi:10.1002/1527-2648(200111)3:11<906::AID-ADEM906>3.0.CO;2-C.

[22] M.I. Nieto, I. Santacruz, R. Moreno, Shaping of dense advanced ceramics and coatings by gelation of polysaccharides, Adv. Eng. Mater. 16 (2014) 637–654. doi:10.1002/adem.201400076.

[23] A.R. Studart, V.C. Pandolfelli, E. Tervoort, L.J. Gauckler, Gelling of Alumina Suspensions Using

Alginic Acid Salt and hydroxylaluminium diacetate, J. Am. Ceram. Soc. 18 (2002) 2711–2718. doi:10.1111/j.1151-2916.2002.tb00518.x.

[24] J. Ma, Z. Xie, H. Miao, B. Zhang, X. Lin, Y. Cheng, Gelcasting of alumina ceramic components in nontoxic Na-alginate–CaIO3–PVP systems, Mater. Des. 26 (2005) 291–296. doi:10.1016/j.matdes.2004.06.011.

[25] A. Islam, Y.H. Taufiq-Yap, P. Ravindra, M. Moniruzzaman, E.-S. Chan, Development of a procedure for spherical alginate–boehmite particle preparation, Adv. Powder Technol. 24 (2013) 1119–1125. doi:10.1016/j.apt.2013.03.021.

[26] S. Mazzitelli, A. Tosi, C. Balestra, C. Nastruzzi, G. Luca, F. Mancuso, et al., Production and characterization of alginate microcapsules produced by a vibrational encapsulation device, J. Biomater. Appl. 23 (2008) 123–45. doi:10.1177/0885328207084958.

[27] V. Nemethova, I. Lacik, F. Razga, Vibration Technology for Microencapsulation : The Restrictive Role of Viscosity, J. Bioprocess. Biotech. 5 (2015) 2014–2016. doi:10.4172/2155-9821.1000199.

[28] D. Serp, E. Cantana, C. Heinzen, U. Von Stockar, I.W. Marison, Characterization of an encapsulation device for the production of monodisperse alginate beads for cell immobilization, Biotechnol. Bioeng. 70 (2000) 41–53. doi:10.1002/1097-0290(20001005)70:1<41::AID-BIT6>3.0.CO;2-U.

[29] Lord Rayleigh, On The Instability Of Jets, Proc. London Math. Soc. s1-10 (1878) 4–13. doi:10.1112/plms/s1-10.1.4.

[30] W. Yu, B.C. Hancock, Evaluation of dynamic image analysis for characterizing pharmaceutical excipient particles, Int. J. Pharm. 361 (2008) 150–7. doi:10.1016/j.ijpharm.2008.05.025.

[31] A.M. Bouwman, J.C. Bosma, P. Vonk, J.H. a. Wesselingh, H.W. Frijlink, Which shape factor(s) best describe granules?, Powder Technol. 146 (2004) 66–72.

doi:10.1016/j.powtec.2004.04.044.

[32] P. Smrdel, The Influence of Selected Parameters on the Size and Shape of Alginate Beads Prepared by Ionotropic Gelation, Sci. Pharm. 76 (2008) 77–89. doi:10.3797/scipharm.0611-07.

[33] AxioVision User's guide, Göttingen, Germany, 2012.

[34] M. Li, D. Wilkinson, K. Patchigolla, Comparison of Particle Size Distributions Measured Using Different Techniques, Part. Sci. Technol. 23 (2005) 265–284. doi:10.1080/02726350590955912.

[35] C. Couroyer, M. Ghadiri, P. Laval, N. Brunard, F. Kolenda, Methodology for Investigating the Mechanical Strength of Reforming Catalyst Beads, Oil Gas Technol. 55 (2000) 67–85.

[36] T. Ferreira, W. Rasband, ImageJ User Guide, Bethesda, Maryland, USA, 2012.

[37] L. Martinez, F. Agnely, R. Bettini, M. Besnard, P. Colombo, G. Couarraze, Preparation and characterization of chitosan based micro networks: Transposition to a prilling process, J. Appl. Polym. Sci. 93 (2004) 2550–2558. doi:10.1002/app.20785.

[38] T. SAKAI, N. HOSHINO, Production of uniform droplets by longitudinal vibration of audio frequency., J. Chem. Eng. Japan. 13 (1980) 263–268. doi:10.1252/jcej.13.263.

[39] B. Singh, D.K. Sharma, R. Kumar, A. Gupta, Development of a new controlled pesticide delivery system based on neem leaf powder, J. Hazard. Mater. 177 (2010) 290–299. doi:10.1016/j.jhazmat.2009.12.031.

[40] Almatis, Reactive Aluminas for Ceramic Applications, (n.d.) 1–2.

[41] C. Domínguez, J. Chevalier, R. Torrecillas, G. Fantozzi, Microstructure development in calcium hexaluminate, J. Eur. Ceram. Soc. 21 (2001) 381–387. doi:10.1016/S0955-2219(00)00143-6.

[42] D. Asmi, I.M. Low, Physical and mechanical characteristics of in-situ alumina/calcium hexaluminate composites, J. Mater. Sci. Lett. 17 (1998) 1735–1738.

doi:10.1023/A:1006683421321.

[43] D. a. Jerebtsov, G.G. Mikhailov, Phase diagram of CaO-Al2O3 system, Ceram. Int. 27 (2001) 25–28. doi:10.1016/S0272-8842(00)00037-7.

[44] M.K. Cinibulk, Effect of Precursors and Dopants on the Synthesis and Grain Growth of Calcium Hexaluminate, J. Am. Ceram. Soc. 81 (1998) 3157–3168. doi:10.1111/j.1151-2916.1998.tb02751.x.

[45] A. Altay, M.A. Gülgün, Microstructural Evolution of Calcium-Doped α-Alumina, J. Am. Ceram. Soc. 86 (2003) 623–29. doi:10.1111/j.1151-2916.2003.tb03349.x.

[46] D. Asmi, I.M. Low, Self-reinforced Ca-hexaluminate/alumina composites with graded microstructures, Ceram. Int. 34 (2008) 311–316. doi:10.1016/j.ceramint.2006.10.001.

Supplementary data

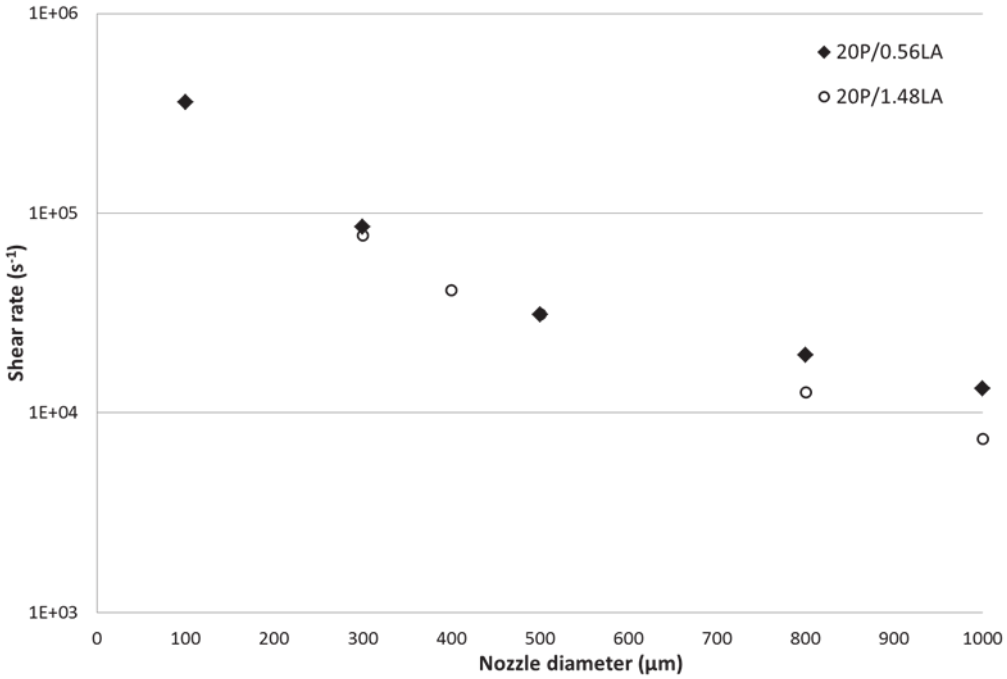

Figure A: Shear rate in function of nozzle radius

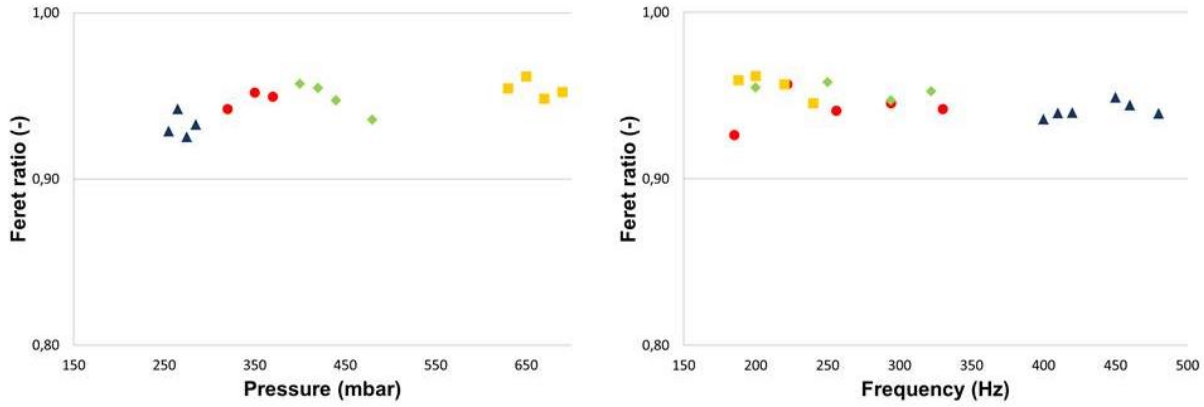

Figure B: Influence of process variables on feret ratio of wet alumina microspheres using different suspensions and a 500 µm nozzle at A: constant frequency of 300 Hz and B: constant pressure of 350 mbar. 40P/0.66LA (green diamond), 20P/1.48HA (yellow square), 20P/0.88HA (red dot), 20P/0.88LA (blue triangle).

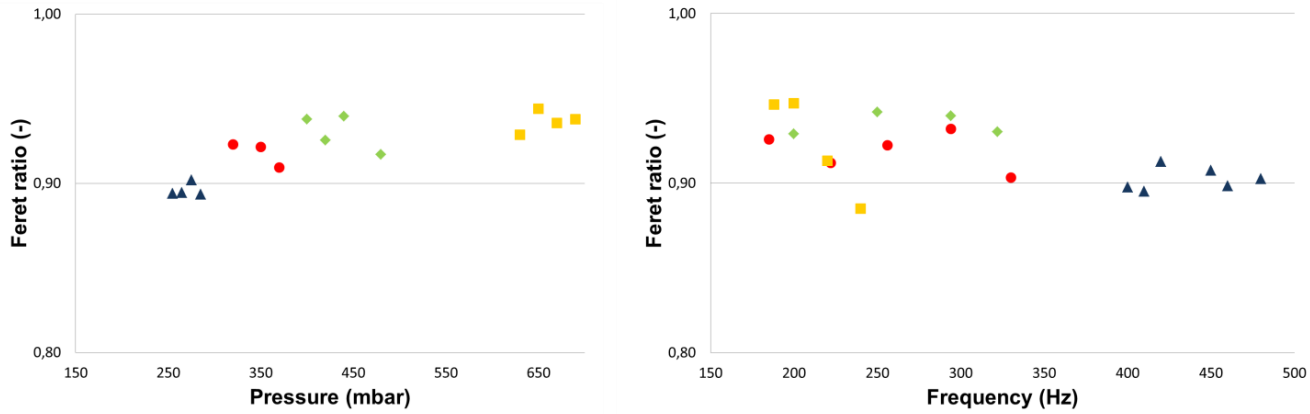

Figure C: Influence of process variables on feret ratio of dry alumina microspheres using different suspensions and a 500 µm nozzle at A: constant frequency of 300 Hz and B: constant pressure of 350 mbar. 40P/0.66LA (green diamond), 20P/1.48HA (yellow square), 20P/0.88HA (red dot), 20P/0.88LA (blue triangle).

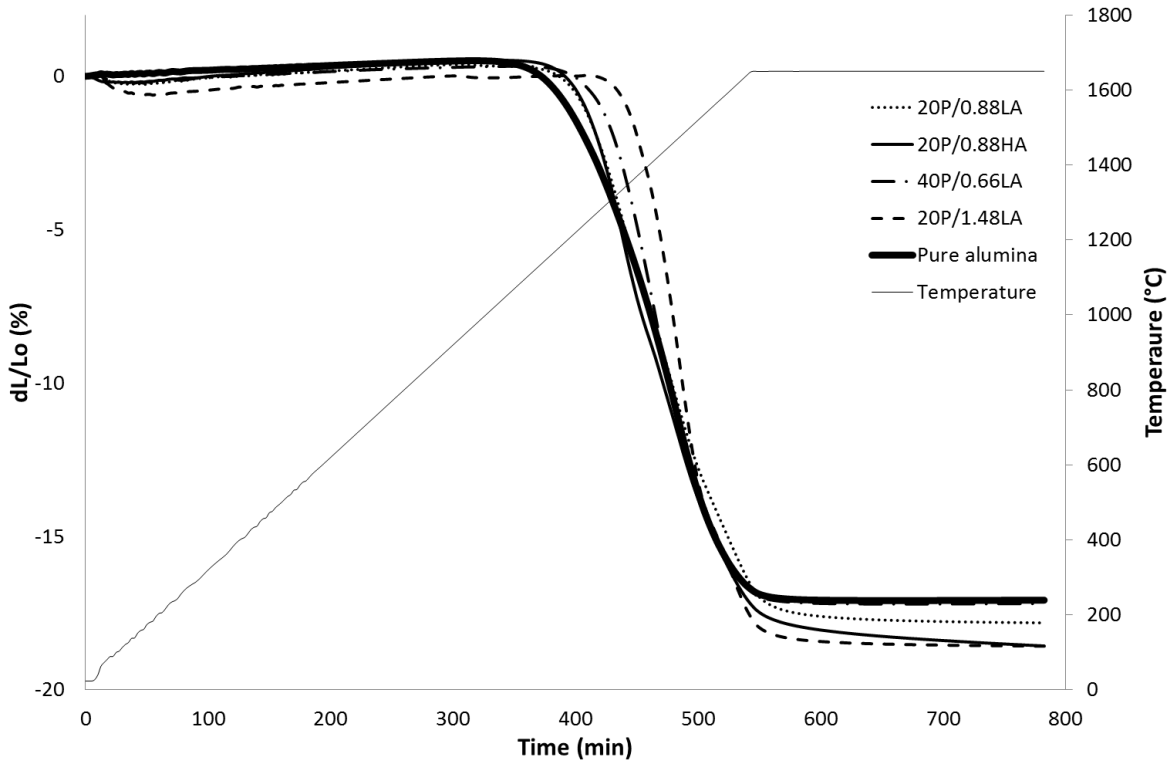

Figure D: Dilatometry data in function of time and temperature of pellets prepared from the four suspensions and pure alumina.

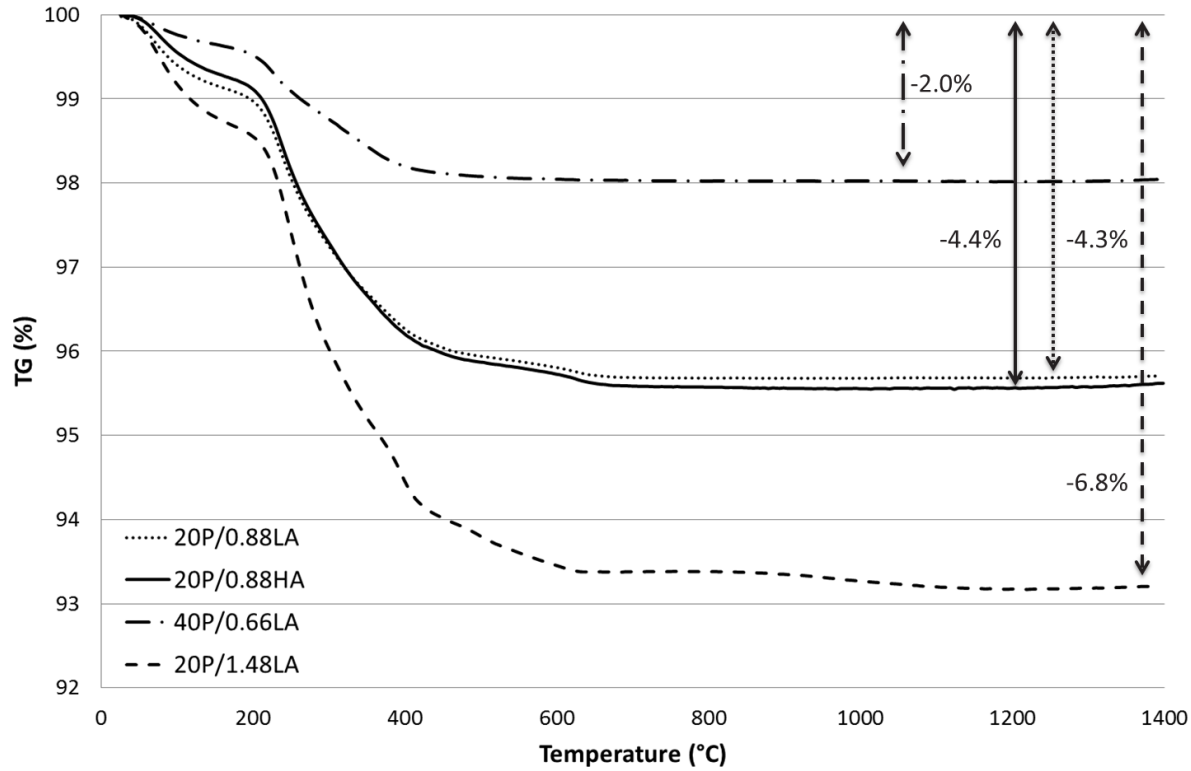

Figure E: Thermogravimetric data (TG) of the four suspensions with total weight loss at 1400 °C

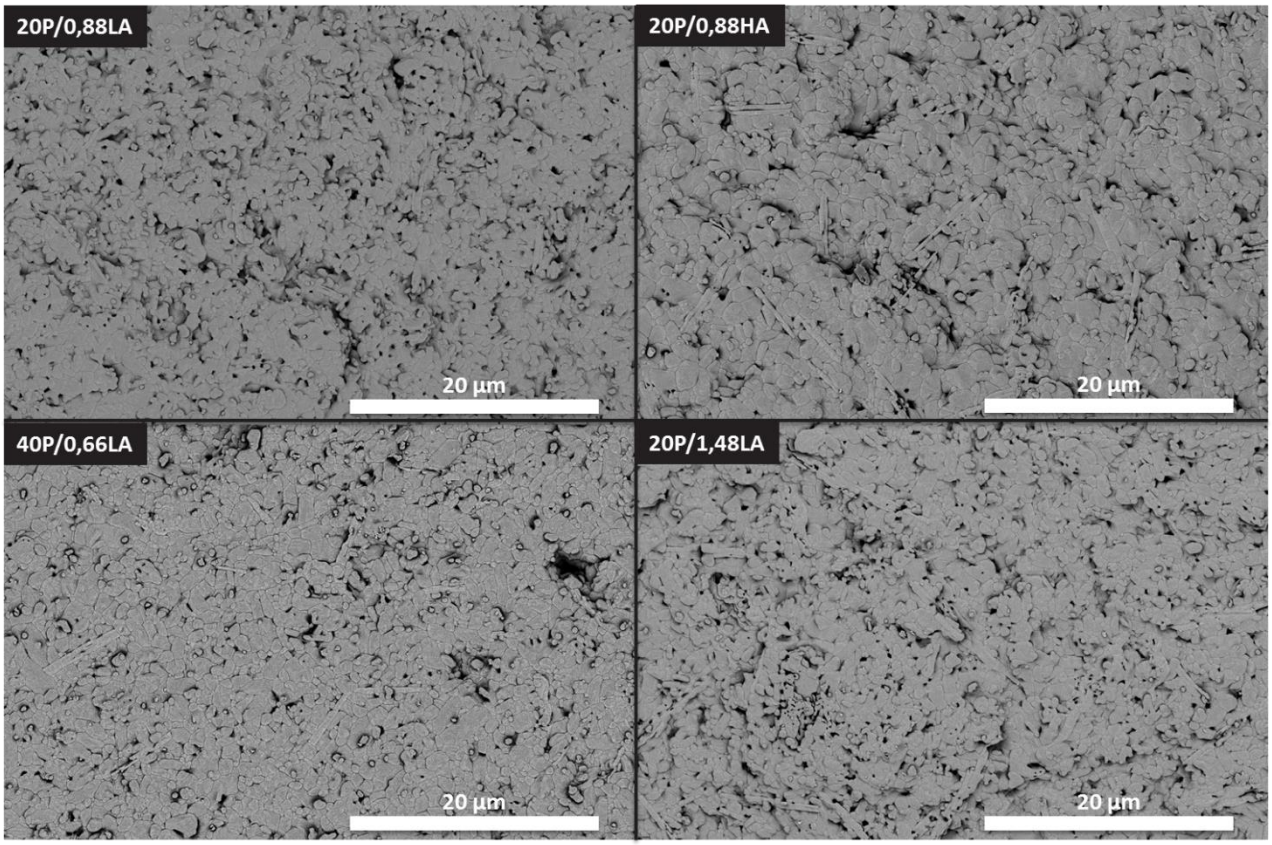

Figure F: SEM image of the microstructure on the surface of the alumina microspheres.

(Sintered 1h @ 1650 °C)